



NJC

Competition between hydrogen bonds and halogen bonds: A structural study

Journal:	<i>New Journal of Chemistry</i>
Manuscript ID	NJ-ART-01-2018-000537.R1
Article Type:	Paper
Date Submitted by the Author:	28-Mar-2018
Complete List of Authors:	Gamekkanda , Janaka ; Kansas State University, Chemistry Sinha, Abhijeet; Kansas State University, Department of Chemistry Desper, John; Kansas State University, Chemistry Đaković, Marijana; University of Zagreb, Department of Chemistry Aakeröy, Christer; Kansas State University, Chemistry

SCHOLARONE™
Manuscripts



Journal Name

ARTICLE

Competition between hydrogen bonds and halogen bonds: A structural study

Janaka C. Gamekkanda,^a Abhijeet S. Sinha,^a John Desper,^a Marijana Đaković,^b and Christer B. Aakeröy^{*a}

Received 00th January 20xx,
Accepted 00th January 20xx

DOI: 10.1039/x0xx00000x

www.rsc.org/

The competition and balance between intermolecular hydrogen bonds (HBs) and halogen bonds (XBs) were explored by co-crystallizing tetra-functionalized (2 x HB (-OH) and 2 x XB (-C≡C-I)) molecules, *trans*-1,4-*bis*(iodoethynyl)cyclohexane-1,4-diol (**D1**) and *cis*-1,4-*bis*(iodoethynyl)cyclohexane-1,4-diol (**D2**), with six ditopic nitrogen based acceptors molecules. Crystal structures of both **D1** and **D2** showed non-covalent interactions between HB/XB donors and available acceptor sites (oxygen/ triple bond/ negative region of iodine). In three co-crystals of **D1** the HB and XB donors act in similar ways as both activated iodine and hydroxyl hydrogen bind to the nitrogen acceptors in the solid state. In contrast, in a co-crystal of **D2**, a geometric isomer of **D1**, there were only hydrogen bonds to the co-former and the halogen-bond donor interacted with the hydroxyl oxygen atoms of **D2**. A stronger tendency for linear XB interactions (as well as greater van der Waals radii reduction) were observed with nitrogen atoms as acceptors (average reduction = 23%) compared to those involving an oxygen atom as an acceptor (average reduction = 16%). A control molecule, *trans*-1,4-diethynylcyclohexane-1,4-diol (**D3**) which has only HB donors (-OH and -C≡C-H) was also examined to get a better understanding of the balance between XB and HB interactions. The ethynyl hydrogen atom did not form hydrogen bonds to the nitrogen atoms in acceptors, and only O-H...N and -C≡C-H...O hydrogen bonds were observed in these structures.

In order to develop practical and robust strategies for efficient synthesis of co-crystals,¹ it is helpful to employ intermolecular interactions that can provide a hierarchical assembly protocol.^{2, 3} By combining interactions that do not compete for the same molecular binding sites it is, in principle, possible to avoid or at least minimize “synthon cross-over”⁴ thereby producing architectures of considerable complexity.⁵⁻⁸ For some time, the hydrogen bond (HB) has been the preeminent synthetic tool in this arena,⁹⁻¹² but the halogen bond (XB) has also received much attention as a vehicle for synthesis and directed assembly of supramolecular heteromeric architectures.¹³⁻¹⁸ Both interactions are directional and relatively strong, and their importance in crystal engineering, originates with their shared dependence upon long-range electrostatic forces.¹⁹⁻²³ Interestingly, several cases of solid-state HB/XB mimicry have been reported where an acceptor site (electron-pair donor) forms structurally identical interactions with both HB and XB donors.²⁴ For example, the hydrogen-bond donor hydroquinone plays the same supramolecular role when interacting with 4,4'-bipyridine²⁵ as do iodine, 1,4-diiodobenzene,²⁶ and 1,4-diiodotetrafluorobenzene,²⁷ respectively. Structurally similar interactions are found in co-crystals of tetramethylpyrazine with both 1,4-diiodotetrafluorobenzene²⁸ and with hydroquinone,²⁹ and aminopyrimidine-based ethynyl and iodoethynyl donors form equivalent architectures with

tetramethylpyrazine and 1,2-*bis*(4-pyridyl)ethylene.³⁰ A small number of studies have also explored competition between these interactions through experimental³¹⁻³³ and theoretical³⁴ means, by affixing a HB and an XB donor on the same molecular backbone. In addition, competition between separate XB and HB donors for the same acceptor, *e.g.* mixtures of 1,2-*bis*(4-pyridyl)-ethane, 1,4-diiodotetrafluorobenzene and hydroquinone,²⁷ or of N,N,N',N'-tetramethylethylenediamine, 1,2-diiodo-tetrafluoroethane and ethylene glycol,²⁷ or bi-functional molecules including 4-iodotetrafluorobenzoic acid, 4-iodotetrafluorophenol and 4-iodotetrafluoroaloxime with acceptors such as 4,4'-azobipyridine³⁵ have been reported. The fact that hydrogen bonding and halogen bonding have shared origins means that if we are to advance supramolecular synthesis, we need to learn more about the balance between them in systems where they are likely to compete for the same acceptor sites.

The strength of an XB donor can be enhanced through the addition of electron-withdrawing substituents, but a similar effect can also be achieved by positioning the halogen atom next to an *sp*-hybridized carbon atom,^{26, 36} Despite the increasing popularity of this route for creating powerful XB donors,³⁷ only a limited amount of work has been done on the potential competition between such XB donors and HB donors. To remedy this lack of experimental data, we synthesized two tetra-functionalized molecules and subjected them to co-crystallization experiments with six different acceptors; *trans*-1,4-*bis*(iodoethynyl)cyclohexane-1,4-diol (**D1**) and *cis*-1,4-

^a Department of Chemistry, Kansas State University, Manhattan, KS, 66506, USA.

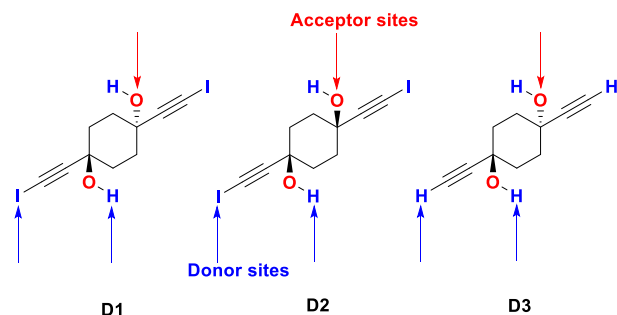
^b Department of Chemistry, Faculty of Science, University of Zagreb, Horvatovac 102a, HR-10000 Zagreb, Croatia.

Electronic Supplementary Information (ESI) available: CCDC 1820020-1820028. TGA, DSC, and crystallographic data. See DOI: 10.1039/x0xx00000x

ARTICLE

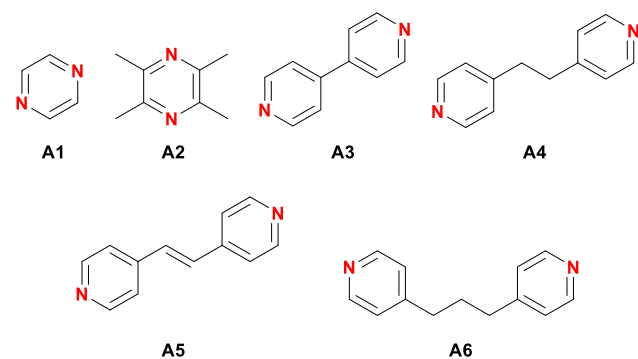
Journal Name

bis(iodoethynyl)cyclohexane-1,4-diol (**D2**) which are geometric isomers of each other are equipped with two HB- and two XB donors, respectively, Scheme 1. In addition, we also explored the structural chemistry of *trans*-1,4-diethynylcyclohexane-1,4-diol (**D3**) which has two pairs of competing HB donors on the same cyclohexane framework.



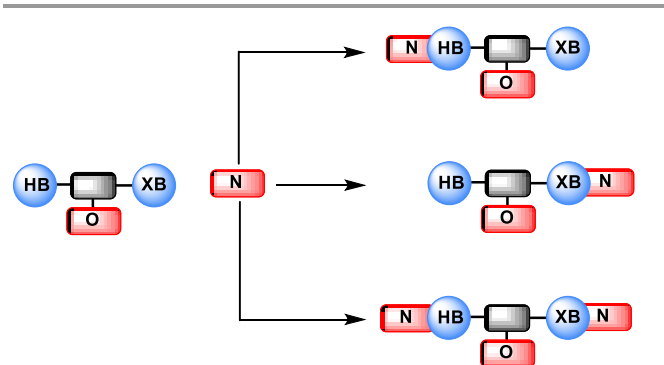
Scheme 1. Probe molecules with competing halogen- and hydrogen-bond donors (**D1/D2**) and competing hydrogen-bond donors (**D3**).

The XB donors in **D1/D2** are “activated” by an *sp*-hybridized carbon atom, and **D3** acts as a control molecule where the XB donor, R-C≡C-I, has been replaced with a geometrically identical HB donor, R-C≡C-H. Two different isomers of the XB donor (*trans/cis*) were prepared in order to explore whether/how molecular geometry would affect synthon preferences. All six acceptor molecules in this study were symmetric ditopic N-heterocyclic compounds, Scheme 2.

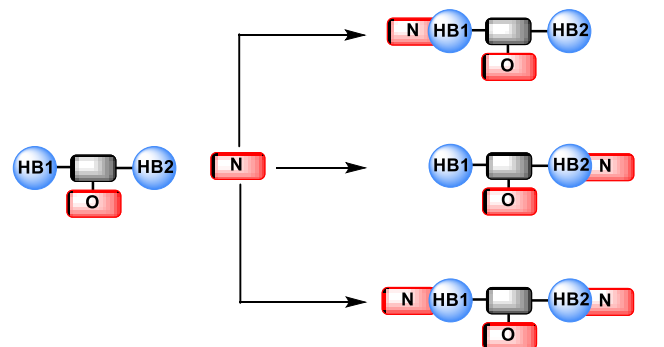


Scheme 2. Six ditopic XB and HB acceptors.

Given the specific combination of donor- and acceptor molecules investigated herein, we hypothesised a series of different outcomes if **D1-D3** were to form co-crystals with the N-heterocyclic acceptors **A1-A6**, Schemes 3 and 4.



Scheme 3. Postulated primary intermolecular interactions in co-crystals of **D1/D2**:**A1-A6**.



Scheme 4. Postulated intermolecular interactions in co-crystals of **D3**:**A1-A6**.

By having the competing halogen- and hydrogen-bond donors on the same molecular backbone, the results are not going to be affected by potential solubility differences which could come into play if the donors were residing on different molecules. Since both XB and HB interactions are dependent upon electrostatic features, we complemented the structural study with an analysis of calculated molecular electrostatic potential surfaces for **D1-D3** in order to try rationalise the outcome of the co-crystallizations. Through these complementary approaches we hoped to shed more light on the supramolecular competition and balance between the two most common synthetic tools in current crystal engineering.

Experimental section

Materials and methods

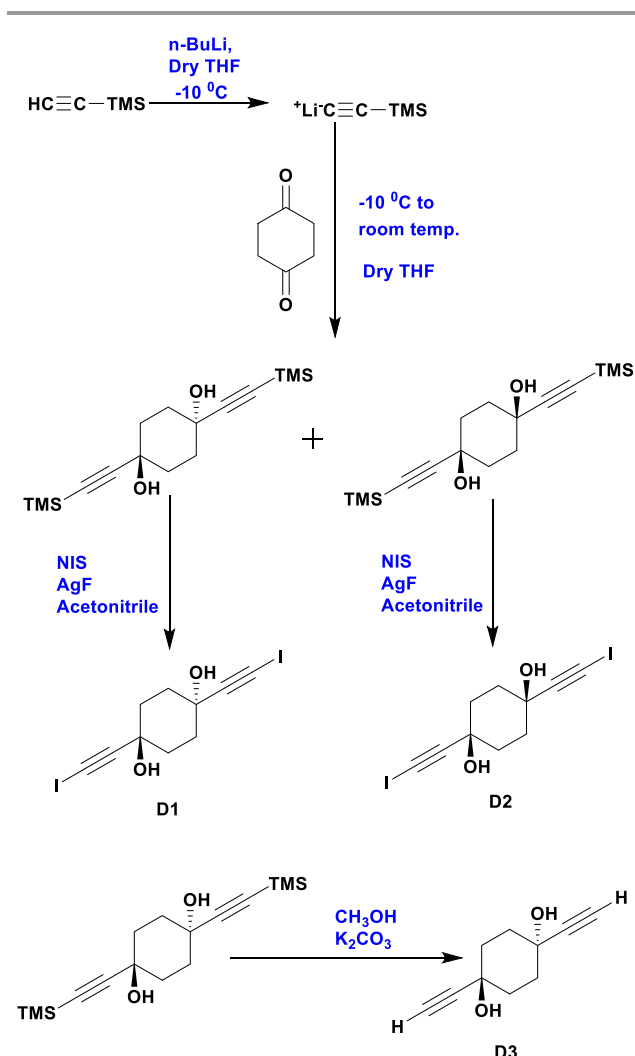
All solvents, reagents, precursors and acceptors (**A1-A6**) were purchased from commercial sources and used without further purification. Melting points were determined using a Fisher-Johns melting point apparatus and are uncorrected. Infrared spectra were obtained on a Nicolet 380 FT-IR spectrometer (optical resolution 0.9 cm^{-1}). ^1H NMR spectra were obtained on a Varian unity plus 400 MHz spectrometer. DSC data were obtained on a TA instruments Q20 and TGA data on a TA instruments Q50.

Computational studies

Starting geometries of the molecules were obtained using the Merck Molecular Mechanics Force Field. All subsequent calculations were carried out using B3LYP functional and 6-31G* basis set which employs LANL2DZ³⁸ under vacuum in Spartan'14 software.³⁹ Molecular electrostatic potential surfaces were generated for the optimized structures on the electron isodensity surface of the 0.002 electrons/au³.

Synthesis of D1-D3

The three donors were synthesized using commercially available 1,4-cyclohexanedione. The ketone was converted to the propargyl alcohol with a TMS protected alkyne group⁴⁰ (the *trans*-cyclohexane being the major product). **D3** was obtained by deprotecting the ethynyl group and **D1** and **D2** were obtained through a reaction with N-iodosuccinimide, Scheme 5.



Scheme 5. Overview of the synthesis of D1-D3.

Synthesis of *trans*- and *cis*-1,4-*bis*((trimethylsilyl)ethynyl)cyclohexane-1,4-diol

A solution of trimethylsilylacetylene (1.75 ml, 18 mmol) was stirred in 100 ml of dry THF and cooled to $-10\text{ }^\circ\text{C}$ under N_2 . A solution of $n\text{-BuLi}$ (4.9 ml, 18 mmol) was added slowly over 30 min. at $-10\text{ }^\circ\text{C}$ under N_2 . The mixture was stirred for an additional hour at the same temperature. Cyclohexane-1,4-dione (1.0 g, 8.9 mmol) was dissolved in 25 ml of dry THF and added dropwise to the resulting trimethylsilyl acetylide solution under N_2 at $-10\text{ }^\circ\text{C}$. The mixture was then allowed to reach room temperature and stirred overnight. After completion of the reaction, 100 ml of water was added and extracted with ethyl acetate ($3 \times 100\text{ ml}$). The combined organic layers were dried over magnesium sulfate and the solution was concentrated to obtain a crude solid and purified by column chromatography. The *trans* isomer was obtained using hexane as the eluent and the *cis* isomer was obtained using a mixture of hexanes: ethyl acetate (8:2) as the eluent. Yield: *trans* isomer 1.43 g, 52%, m.p.: $160\text{-}163\text{ }^\circ\text{C}$, $^1\text{H NMR}$ (400 MHz in DMSO-d_6): 5.43 (2H, s), 1.77-1.62 (8H, m), 0.13 (18H, s) *cis* isomer 0.410 g, 15%, m.p.: $123\text{-}125\text{ }^\circ\text{C}$, $^1\text{H NMR}$ (400 MHz in DMSO-d_6): 5.31 (2H, s), 1.68-1.71 (8H, m), 0.12 (18H, s).

Synthesis of *trans*-1,4-*bis*(iodoethynyl)cyclohexane-1,4-diol.H₂O (D1.H₂O)

Silver fluoride (0.825 g, 6.5 mmol) and *trans*-1,4-*bis*((trimethylsilyl)ethynyl)cyclohexane-1,4-diol (1.0 g, 3.24 mmol) were dissolved in 50 ml of acetonitrile and N_2 was bubbled through the solution for 20 minutes. N-iodosuccinimide (1.46 g, 6.5 mmol) was added to the mixture and the flask was covered with aluminum foil. The reaction was stirred overnight under N_2 . After completion of the reaction, the resulting mixture was passed through a short pad of silica and the resulting solution was evaporated under vacuum in order to get the crude product. It was dissolved in methanol and water was added to the mixture. The product crashed out and the precipitate was filtered and dried in air to give a light-yellow solid. Yield 1.23 g, 87%, m.p.: $218\text{-}220\text{ }^\circ\text{C}$ (dec.), $^1\text{H NMR}$ (400 MHz in DMSO-d_6): 5.57 (2H, s), 1.60-1.80 (8H, m).

Synthesis of *cis*-1,4-*bis*(iodoethynyl)cyclohexane-1,4-diol (D2)

The synthesis of *cis*-1,4-*bis*(iodoethynyl)cyclohexane-1,4-diol was carried out in the same way as the synthesis of **D1** by using 0.250 g (2.0 mmol) of silver fluoride, and 0.3 g (9.7 mmol) of *cis*-1,4-*bis*((trimethylsilyl)ethynyl)cyclohexane-1,4-diol and 0.450 g (2.0 mmol) of N-iodosuccinimide dissolved in 30 ml of acetonitrile. Yield: 0.360 g, 89%, m.p.: $168\text{-}171\text{ }^\circ\text{C}$ (dec.), $^1\text{H NMR}$ (400 MHz in DMSO-d_6): 5.40 (2H, s), 1.61-1.71 (8H, m).

Synthesis of *trans*-1,4-diethynylcyclohexane-1,4-diol.H₂O (D3.H₂O)

Trans-1,4-*bis*((trimethylsilyl)ethynyl)cyclohexane-1,4-diol (0.5 g, 1.6 mmol) and potassium carbonate (0.45 g, 3.25 mmol) were dissolved in 50 ml of methanol. The reaction mixture was stirred for 4 hrs and after completion of the reaction, the solvent was evaporated under vacuum. The solid mixture was dissolved in ethyl acetate and washed with brine. The organic layer was dried over magnesium sulfate and the solvent was evaporated to get a white powder as the product. Yield 0.22 g,

ARTICLE

Journal Name

75%, m.p.: 175-178 °C, ^1H NMR (400 MHz in DMSO- d_6): 5.40 (2H, s), 3.28 (2H, s), 1.61-1.71 (8H, m).

Crystal growth of D1-D3 and synthesis of co-crystals

D1-D3 (10 mg) were individually combined with each acceptor (**A1-A6**) in a 1:1 stoichiometric ratio using solvent assisted grinding (methanol as the solvent). Eighteen experiments were performed and the resulting solids were analysed using IR spectroscopy. The solid mixtures obtained from grinding experiments were dissolved in 2 ml of methanol or methanol/tetrahydrofuran and kept in small vials for slow evaporation at room temperature. Crystals suitable for single-crystal X-ray diffraction were obtained after 2-3 days.

Results

D1 and **D3** crystallized as monohydrates, whereas **D2** did not include any solvent in its lattice. These results were confirmed by TGA, which show the loss of one equivalent of water for both **D1** and **D3** (but not for **D2**), and DSC, which indicate thermodynamic events at the matching temperatures for **D1** and **D3** (ESI).

The relevant maximum positive and negative values on the electrostatic potential surfaces for **D1** and **D3** are listed in Figure 1 (a) and Figure 1 (b) respectively, for **D2** they are listed in Figure 2.

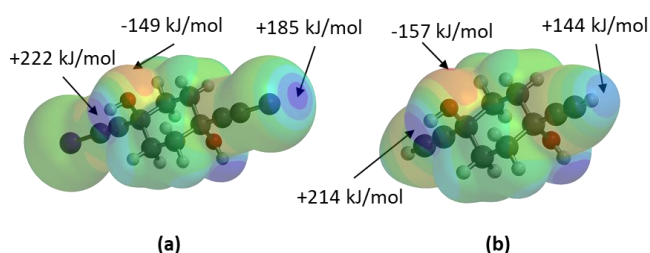


Figure 1. Electrostatic potential surfaces of (a) XB/HB donors and acceptors of **D1**, (b) HB donors and acceptors of **D3**.

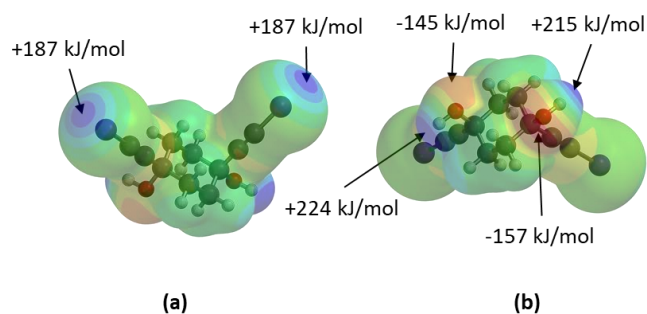


Figure 2. Electrostatic potential surfaces of (a) XB donors, (b) HB donors and XB/HB acceptors of **D2**.

MEPs of **A1-A6** were calculated in order to rank the ability of these molecules to act as HB/XB acceptors (Figure 3).

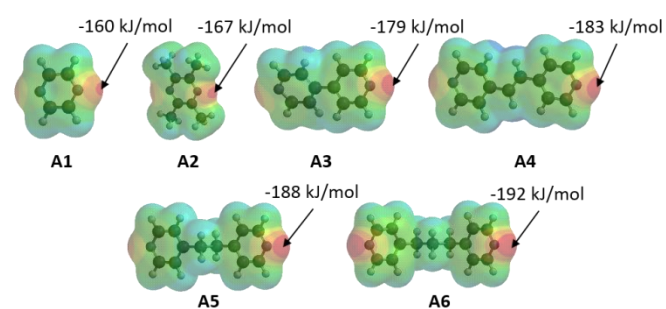


Figure 3. Electrostatic potential surfaces of acceptor atoms in **A1-A6**.

D1-D3 and six co-crystals thereof produced crystals suitable for single-crystal X-ray diffraction, and the crystallographic data is provided in the ESI. Atomic displacement parameters (ADPs) and labelling schemes for all crystals structures are shown in Figure 4.

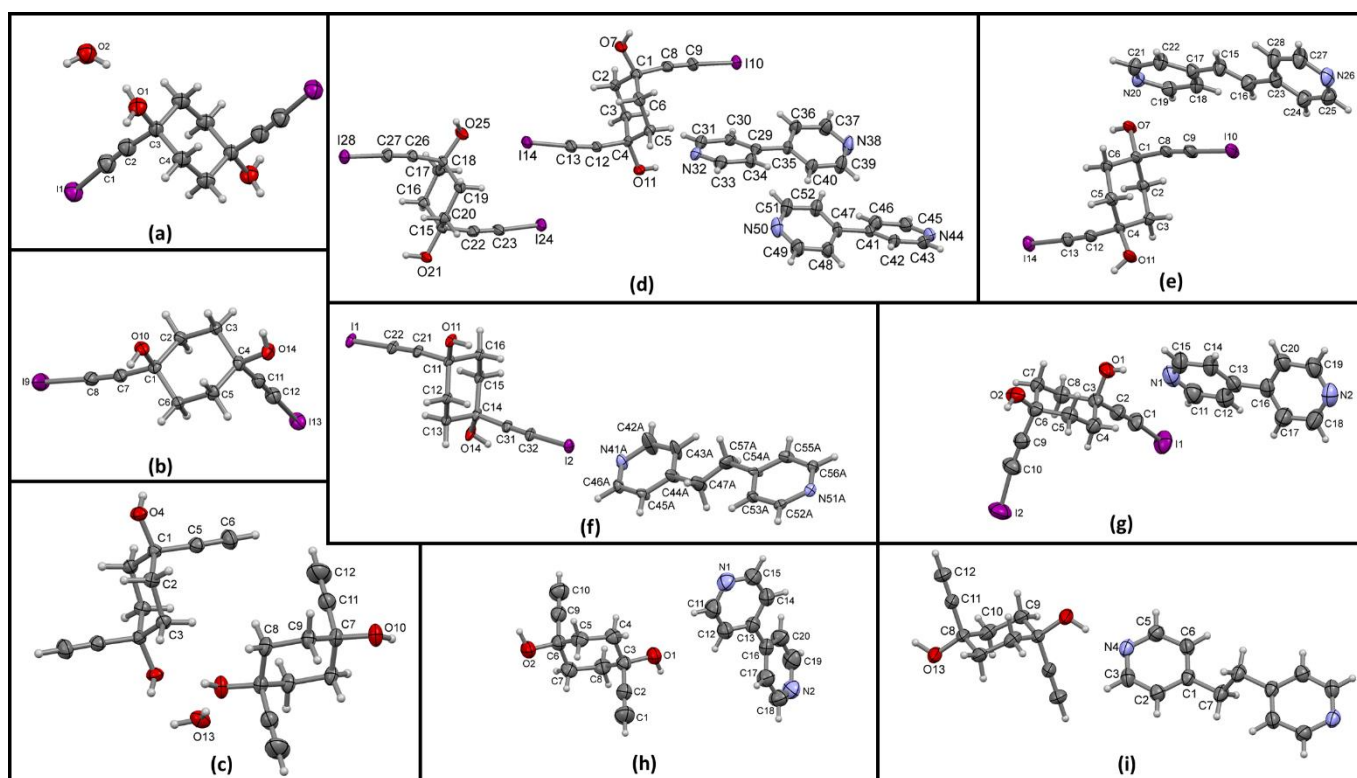


Figure 4. ADPs for crystal structures (a) **D1.H₂O**, (b) **D2**, (c) **D3.H₂O**, (d) **D1:A3**, (e) **D1:A4**, (f) **D1:A5**, (g) **D2:A3**, (h) **D3:A3**, and (i) **D3:A5** (Thermal ellipsoids of crystals are displayed at the 50% probability level).

Geometric parameters for hydrogen- and halogen bonds in the crystal structures of **D1-D3** are given in Table 1 and Table 2, respectively.

Table 1. HB distances and angles in **D1-D3**.

Compound	D-H...A	D...A (Å)	<(DHA) (°)
D1.H₂O	O(1)-H(10)...O(2)	2.8239(19)	164(8)
	O(2)-H(20)...O(1)	2.8239(19)	154(8)
D2	O(10)-H(10)...O(14)	2.806(2)	173(3)
	O(14)-H(14)...O(10)	2.922(2)	170(3)
D3.H₂O	O(4)-H(4)...O(13)	2.6333(11)	173.2(16)
	O(10)-H(10)...O(4)	2.7789(11)	160.8(17)
	O(13)-H(13A)...O(10)	2.7575(13)	168.9(16)
	O(13)-H(13B)...O(4)	2.9174(12)	169.3(18)

Table 2. XB distances and angles in **D1-D2**.

Compound	D-X...A	X...A (Å)	<(DXA) (°)
D1.H₂O	C(1)-I(1)...O(1)	3.146(3)	174.68(15)
D2	C(8)-I(9)...I(13)	3.9222(4)	140.69(7)
	C(12)-I(13)...I(9)	3.9222(4)	71.49(7)
	C(12)-I(13)...C(8)	3.296(2)	168.69(8)
	C(12)-I(13)...C(7)	3.354(2)	170.34(8)

All four donors on **D1** (2 x O-H and 2 x R-C≡C-I) are involved in intermolecular interactions. The intermolecular network is made more complicated by the presence of a water molecule in the lattice. Both XB donors interact with -OH groups of **D1** in a homomeric manner, whereas the hydroxylic HB donors bind to the oxygen atoms of water. The disordered water molecule acts as a hydrogen bond donor to the hydroxylic oxygen atoms of **D1**, Figure 5.

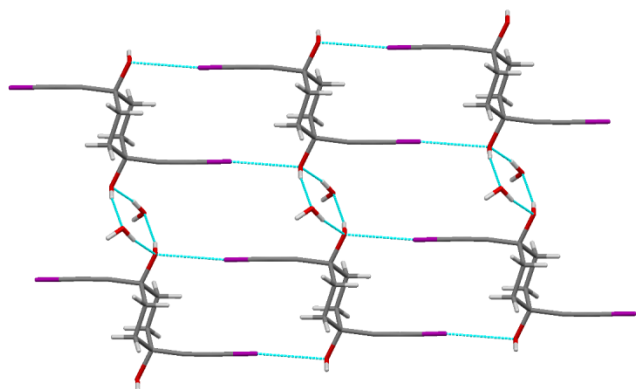


Figure 5. Hydrogen bonding and halogen bonding in the crystal structure of **D1.H₂O**.

In the crystal structure of **D2**, there are two intermolecular hydrogen bonds between adjacent hydroxyl groups, (Figure 6a). In addition, there is one XB involving the triple bond of **D2** as an acceptor site $r(I \cdots \text{centroid of triple bond})$ ca. 3.27 Å, $\theta(\text{centroid of triple bond} \cdots I-C)$ ca. 177.76°, and one iodine...iodine type II interaction, (Figure 6b).

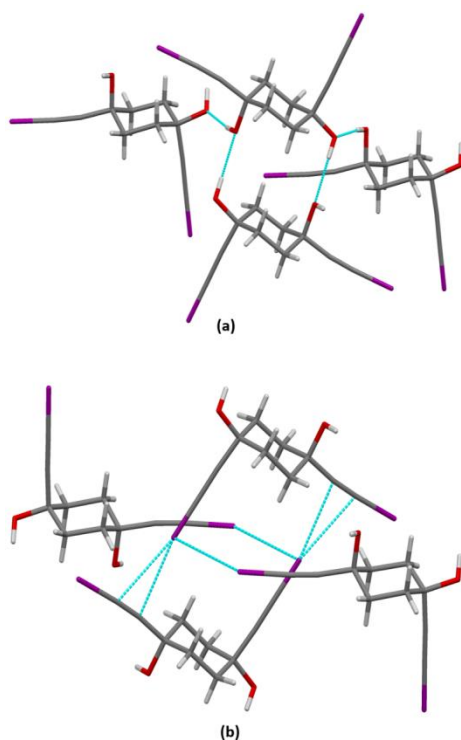


Figure 6. Hydrogen bonds (a) and halogen bonds (b) in the crystal structure of **D2**.

In the crystal structure of **D3.H₂O**, there are **D3...D3** water-bridged interactions (Figure 7a) as well as direct **D3...D3** hydrogen bonds (Figure 7b), and a triple bond...ethynyl hydrogen atom interaction $r(C \cdots \text{centroid of triple bond})$ ca. 3.87 Å, $\theta(\text{centroid of triple bond} \cdots H-C)$ ca. 138° (Figure 7b).

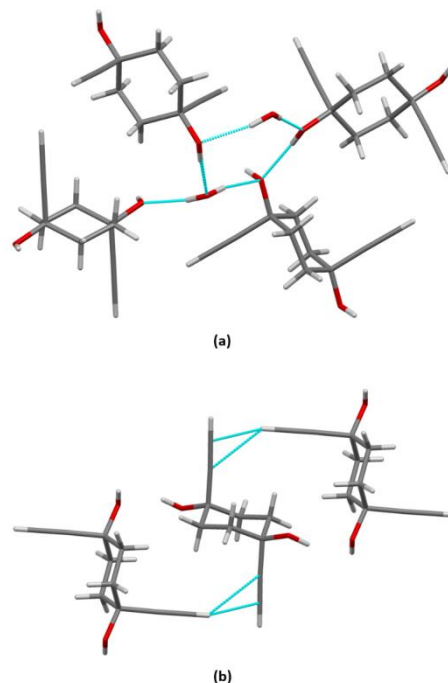


Figure 7. (a) Water bridged hydrogen bonding and (b) C-H...C≡C hydrogen bond in the crystal structure of **D3.H₂O**.

Even though we were only able to determine the crystal structure of six co-crystals using single-crystal X-ray diffraction (Table 3 and Table 4), the IR analysis of the sixteen attempted co-crystallizations found unambiguous evidence for co-crystal formation in each case (see Supplementary data).

Table 3. HB distances and angles in the structures of six co-crystals. (* Some of the hydrogen atoms involved in hydrogen-bonding could not be located based on the difference electron density. Hence, they were placed in geometrically calculated positions and refined using a riding model)

Compound	D-H...A	D...A (Å)	<(DHA) (°)
D1:A3	O(7)-H(7)...O(11)	2.758(5)	159(9)
	O(11)-H(11)...N(32)	2.809(5)	161(7)
	O(21)-H(21)...N(44)	2.786(6)	163(7)
	O(25)-H(25)...O(21)	2.717(5)	171.5*
D1:A4	O(7)-H(7)...N(20)	2.792(3)	172(3)
	O(11)-H(11)...O(7)	2.740(2)	169.(3)
D1:A5	O(11)-H(11)...N(51A)	2.726(7)	172.9*
	O(11)-H(11)...N(51B)	2.831(12)	174.7*
	O(14)-H(14)...O(11)	2.740(3)	168.7*
D2:A3	O(1)-H(10)...N(1)	2.810(7)	165(9)
	O(11)-H(20)...N(2)	2.791(7)	174(7)
D3:A3	O(1)-H(10)...N(2)	2.777(18)	170.5(19)
	O(2)-H(20)...N(1)	2.824(19)	170(2)
	C(10)-H(10)...O(1)	3.303(3)	173(2)
D3:A5	O(13)-H(13)...N(4)	2.731(16)	171(2)
	C(12)-H(12)...O(13)	3.235(2)	160.7*

Table 4. XB distances and angles in the structures of four co-crystals.

Compound	D-X...A	X...A (Å)	<(DXA) (°)
D1:A3	C(9)-I(10)...N(50)	2.826(5)	178.30(19)
	C(13)-I(14)...O(25)	2.938(4)	175.19(19)
	C(23)-I(24)...O(7)	2.951(4)	173.60(19)
	C(27)-I(28)...N(38)	2.782(4)	178.97(19)
D1:A4	C(9)-I(10)...O(11)	2.9273(17)	174.73(8)
	C(13)-I(14)...N(26)	2.768(2)	177.81(9)
D1:A5	C(32)-I(2)...N(41B)	2.755(8)	173.2(5)
	C(32)-I(2)...N(41A)	2.761(4)	179.9(2)
	C(22)-I(1)...O(14)	2.901(2)	175.12(9)
D2:A3	C(1)-I(1)...O(2)	2.978(4)	154.6(2)
	C(10)-I(2)...O(1)	2.955(4)	159.0(2)

In the structure of **D1:A3**, there are two halogen bonds; I...N (a 20% combined vdW reduction) and I...O (a 16% vdW reduction). These interactions are mirrored by two hydrogen bonds, O...N and O...O, respectively, involving the same type of acceptor sites that were participating in halogen bonds, (Figure 8).

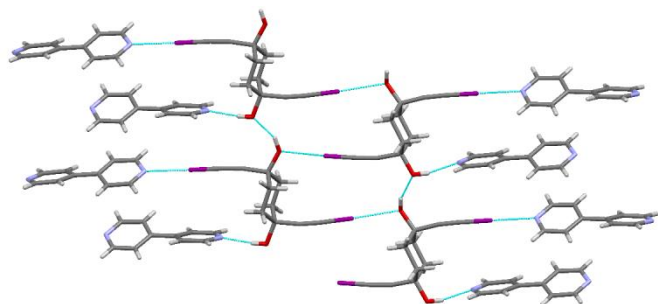


Figure 8. Main HBs and XBs in the crystal structure of **D1:A3**.

The crystal structure of **D1:A4** displays the same set of intermolecular interactions as were found in **D1:A3**. One I...N halogen bond (with a 22% vdW reduction) and one I...O halogen bond (with a 16% vdW reduction). Again, these interactions are mimicked by two hydrogen bonds, O...N and O...O, Table 3, Figure 9.

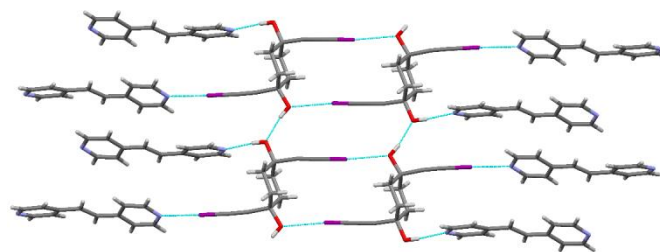


Figure 9. Main HBs and XBs in the crystal structure of **D1:A4**.

In the crystal structure of **D1:A5** we again find the same combination of two halogen bonds (with a 22% and a 17% reduction in the combined vdW radii for I...N and I...O, respectively) and two structurally similar hydrogen bonds, (Figure 10).

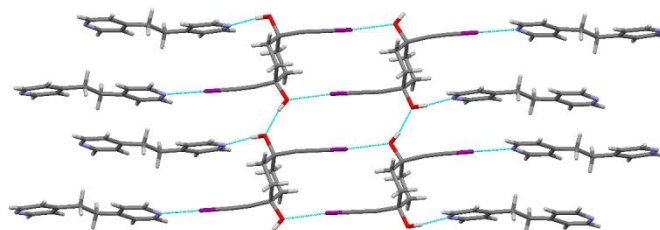


Figure 10. Main HBs and XBs in the crystal structure of **D1:A5**.

Up to this point, all three co-crystals of **D1** contain the same set of hydrogen- and halogen bonds, but when acceptor **A3** is introduced to the geometric isomer **D2**, and different set of interactions are observed. The heteromeric co-crystallization is now driven only by two O...N hydrogen bonds, leaving the two C≡C-I moieties to form halogen bonds to the hydroxylic oxygen atoms (with a 15% vdW reduction) of the molecule to which they are attached, (Figure 11).

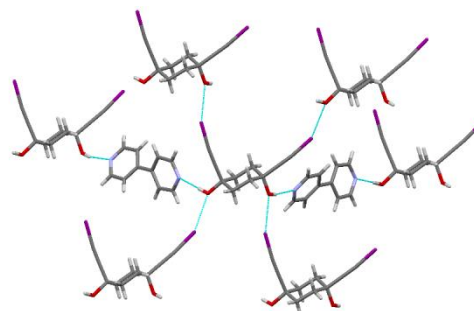


Figure 11. Main HBs and XBs in the crystal structure of **D2:A3**.

In the crystal structure of **D3:A3**, where the C≡C-I moieties have been replaced with C≡C-H groups on **D3**, O-H...N hydrogen bonds are exclusively responsible for the co-crystal formation, accompanied by C≡C-H...O interactions involving the hydroxylic oxygen atoms of **D3**, (Figure 12).

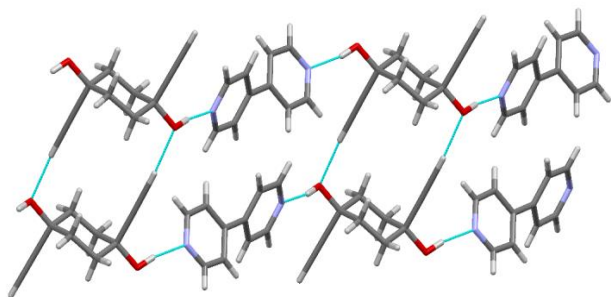


Figure 12. Main HBs in the crystal structure of **D3:A3**.

Finally, in the crystal structure of **D3:A5**, the co-crystal is formed as a result of two O-H...N hydrogen bonds, and this time both ethynyl group form hydrogen bonds with hydroxylic oxygen atoms as acceptor sites, (Figure 13).

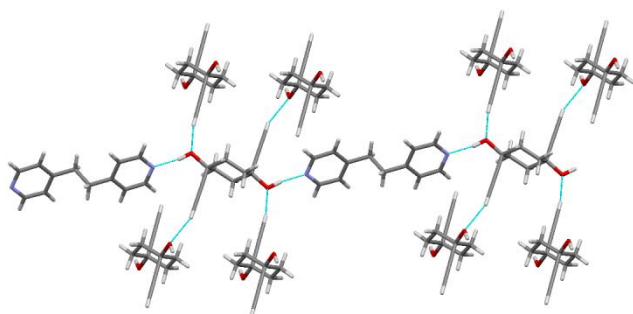


Figure 13. Main HBs in the crystal structure of **D3:A5**.

Discussion

The crystal structure determinations of the three target molecules revealed that both **D1** and **D3** appeared as hydrates in the solid state, whereas crystalline **D2** did not include any additional components. The inclusion of water molecules in the structure **D1** makes it possible for C-I...O(hydroxyl) halogen bonds and O-H...O(water) hydrogen bonds to exist side by side. The lack of water molecules in the structure of **D2**, means that there is a shortage of oxygen acceptor sites and in this case, the competition between O-H and C-I leads to O-H...O hydrogen bonds. The C-I groups have to resort to forming type II halogen bonds to the electron-rich equatorial region of a neighboring iodine atom⁴¹ and also through a side-on contact with a triple bond.⁴² In the structure of **D3.H₂O**, the ethynyl hydrogen atoms also form hydrogen bonds through a side-on interaction with an electron rich area of triple bond in an adjacent molecule of **D3**.⁴³

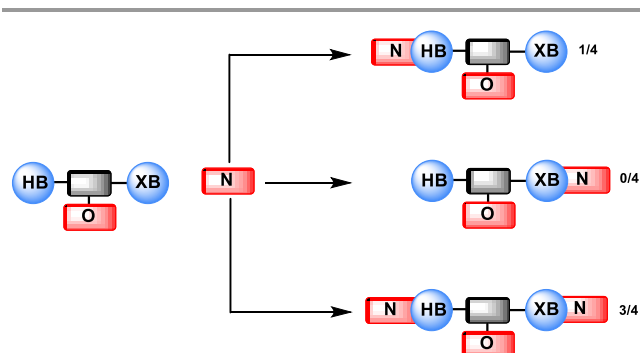
IR spectroscopy is an effective and sensitive method for detecting co-crystal formation.⁴⁴ We observed a red-shift of the O-H peak from *ca.* 3279 cm⁻¹ to 3260 cm⁻¹ with the formation of a co-crystal (**D1:A3**) and a red-shift of the stretch

associated with the triple bond (from *ca.* 2158 cm⁻¹ to 2153 cm⁻¹). Complementary blue-shifts of the acceptors in the **D1:A3** were found (from *ca.* 1586 cm⁻¹ to 1590 cm⁻¹) in 4,4'-bipyridine upon co-crystal formation.⁴⁵

Based on the three co-crystals formed by **D1** with **A3-A5**, respectively, it seems that the XB and HB donors are equally capable of competing for the available acceptor sites even though they have different MEP values. The iodine atom acts in a structurally similar way to the hydrogen atom indicating the close competitiveness between the two and illustrating the difficulty of predicting the outcome solely based on MEP values.⁴⁶ It has been shown previously, that if the Q value (Q = HB electrostatic potential – XB electrostatic potential)³¹ is less than about 140 kJ/mol then the HB and XB donors are likely to be competitive with each other. In **D1** the difference in electrostatic potential between the two donors is 37 kJ/mol which is thus in agreement with earlier studies.

Different relative positioning of the hydroxyl groups in **D2** compared to in **D1** (equatorial:equatorial in **D1** vs axial:equatorial in **D2**) (Figure 1 (a) and Figure 2 (b)) results in slightly different MEPs for hydrogen bond donors (axial OH; 224 kJ/mol, equatorial OH; 215 kJ/mol), making one hydroxyl group a better HB donor than the other. In contrast, even though the two iodine atoms in **D2** are in different geometric orientation (axial and equatorial), they show similar MEPs (187 kJ/mol). This different MEPs of the two O-H hydrogen bond donors are also reflected in the intermolecular bond distances in **D3:A3**, *r*(O axial...N) 2.791(7) Å and *r*(O equatorial...N) 2.810(7) Å (a high MEP value matches with a shorter bond distance, and vice versa). Even though the Q values of the two pairs of XB and HB donors on **D2** are 37 kJ/mol and 28 kJ/mol, respectively, (substantially lower than 140 kJ/mol) the hydrogen-bond donors dominate over the C-I donors in the competition for the best hydrogen-bond acceptor, the hydroxylic oxygen atoms.

In the three co-crystals of **D1**, (with **A3**, **A4**, and **A5**) both XB and HB donors act in comparable ways by each interacting with two nitrogen acceptor sites and two oxygen acceptors. In the one co-crystal of **D2** (which has a *cis*-configuration of donor sites) the HB donor drives the co-crystal synthesis by forming an O-H...N hydrogen bond with bipyridine, which leaves the hydroxylic oxygen atoms to engage with the C-I halogen-bond donors indicating that relatively subtle changes in molecular geometry can tip the balance in favor of one donor over another (Scheme 6). Furthermore, the polarity of the solvent can also play a key role in shifting the balance between HB and XB interactions in a competitive situation.²⁴



Scheme 6. Summary of interactions between HB/ XB donors and nitrogen-based acceptors.

The intermolecular packing in **D1:A3** is different to that found in **D1:A4** and **D1:A5** due to the presence of additional moderate⁴⁷ to weak⁴⁸ $\pi\cdots\pi$ interactions ($r(\pi\cdots\pi)$ 3.83 Å and 3.94 Å) between rings of **A3** (Figure 14). In **D1:A4** and **D1:A5**, it is not possible for the pyridyl rings to stack on top of each other since the bridging groups between rings in **A4** and **A5** necessitates that the aromatic groups end up being sandwiched between the aliphatic bridges of adjacent conformers within each stack, (Figure 9 and Figure 10), once the structure directing hydrogen- and halogen bonds have formed.

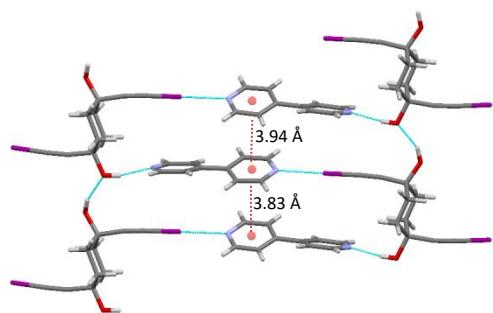
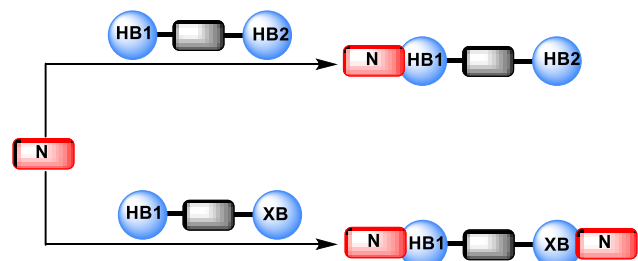


Figure 14. Moderate/weak $\pi\cdots\pi$ stacking in the crystal structure of **D1:A3**.

The ethynyl hydrogen atom is capable of making substantive hydrogen bonds with nitrogen based^{49, 50} or oxygen based⁵¹ acceptors in co-crystallizations. But, in **D3** it cannot compete effectively with the hydroxyl hydrogen (Scheme 7) which indicates that the ethynyl hydrogen is a weaker donor than the ethynyl iodine.



Scheme 7. Competition of halogen bonding with hydrogen bonding in the presence of same acceptor.

Nitrogen acceptors of all co-crystal shows a higher vdW reduction in XB bonding when compared to oxygen acceptors (average vdW radii reduction is 21% for $I\cdots N$, average vdW reduction is 16% for $I\cdots O$). All the XB distances and angles between aromatic nitrogen atoms and ethynyl iodine functionality are in the range of values found among the 44 relevant structures found in the CSD⁵² (Figure 15 and 16). There is only one previously reported structure with an iodo-ethynyl halogen bond involving a hydroxyl oxygen atom $r(I\cdots O)$ *ca.*2.98 Å, $\theta(C-I\cdots O)$ *ca.*178.5°.⁵³

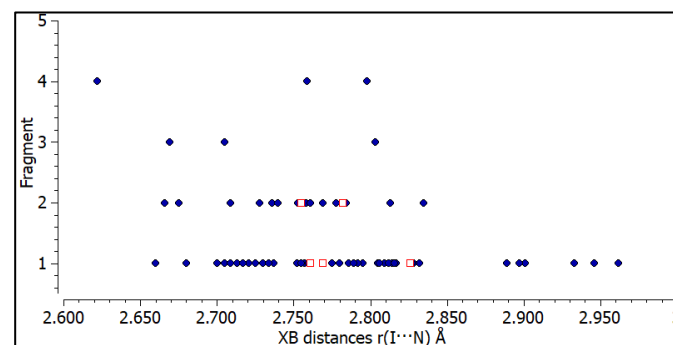


Figure 15. XB distances between ethynyl iodine and aromatic nitrogen: reported in CSD (blue circles) and observed in this study (red hollow squares).

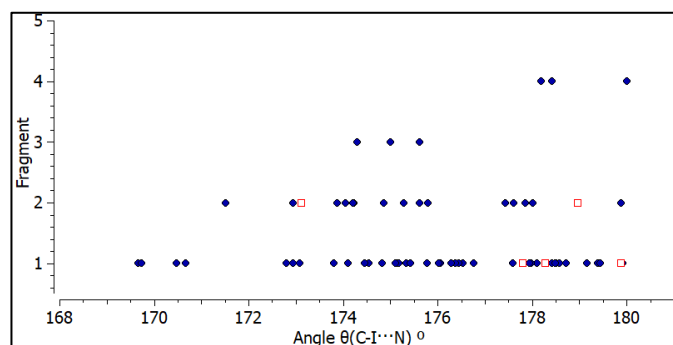


Figure 16. XB angles $\theta(C-I\cdots N)$: reported in CSD (blue circles) and observed in this study (red hollow squares).

The angular dependence of halogen bonds shows a greater tendency towards linearity when nitrogen acceptors are involved (average $\theta(C-I\cdots N)$ *ca.*178°), compared to when oxygen atoms act as acceptor sites (average $\theta(C-I\cdots O)$ *ca.*169°).

Conclusions

Based on structural information on two HB/XB tetrafunctionalized molecules, as well as four co-crystals thereof, it is clear that the ability of R-O-H hydrogen-bond donors and R-C≡C-I halogen bond donors to engage in structure-directing interactions is very finely balanced. By and large, the hydroxylic groups and the iodo-ethynyl groups are equally successful when competing for a limited number of nitrogen-based or oxygen-based acceptor sites. The fact that *trans*-1,4-*bis*(iodoethynyl)cyclohexane-1,4-diol, **D1**, and *cis*-1,4-*bis*(iodoethynyl)cyclohexane-1,4-diol, **D2**, behave differently does however, indicate that the balance between

hydrogen- and halogen bonds be altered by very small changes in molecular conformation. In the control molecule, *trans*-1,4-diethynylcyclohexane-1,4-diol, **D3**, where the activated XB donor was replaced by a relatively weak HB donor, R-C≡C-H, the hydroxylic moiety is now dominant due to its substantially larger positive electrostatic potential on the proton. The use of differences in electrostatic potential values of the HB and XB donor, provides a useful indicator of how the balance between the competing forces will manifest itself in the resulting crystal structure. The structural information presented in this study, coupled with rationalizations of the observed results against a background of calculated molecular electrostatic potentials, offer valuable information that may facilitate the reliable design and synthesis of mutli-component solid-state architectures using a transferable synthetic protocols based on a variety of intermolecular interactions.

Conflicts of interest

There are no conflicts to declare.

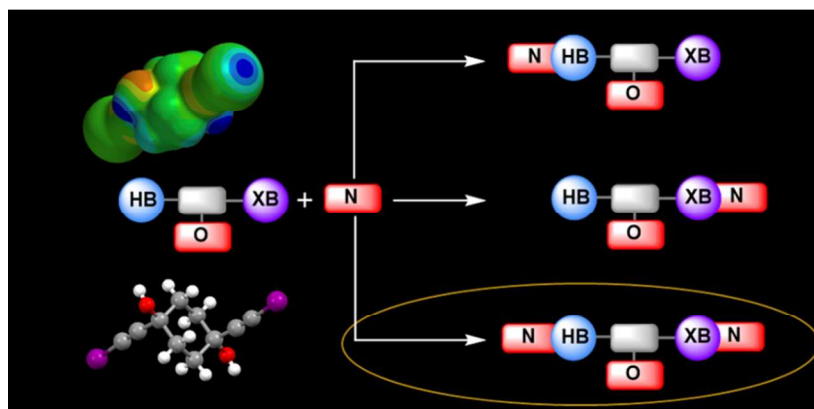
Acknowledgements

This material is based upon work supported by, or in part by, the U. S. Army Research Laboratory and the U. S. Army Research Office under contract/grant number W911NF-13-1-0387 (to C.B.A. and J.C.G) and by the Croatian Science Foundation under project UIP-11-2013-1809 (to M.D). We are also grateful to Dr. V. Day (University of Kansas) for collecting some single-crystal X-ray data.

References

1. C. B. Aakeröy and P. D. Chopade, in *Supramol. Chem.*, John Wiley & Sons, Ltd, 2012, DOI: 10.1002/9780470661345.smc113.
2. C. Rest, R. Kandanelli and G. Fernandez, *Chem. Soc. Rev.*, 2015, **44**, 2543-2572.
3. M. J. Webber, E. A. Appel, E. W. Meijer and R. Langer, *Nat Mater*, 2016, **15**, 13-26.
4. C. B. Aakeröy, P. D. Chopade and J. Desper, *Cryst. Growth Des.*, 2011, **11**, 5333-5336.
5. H. R. Khavasi and A. A. Tehrani, *CrystEngComm*, 2013, **15**, 5813-5820.
6. D. A. Adsmond, A. S. Sinha, U. B. R. Khandavilli, A. R. Maguire and S. E. Lawrence, *Cryst. Growth Des.*, 2016, **16**, 59-69.
7. T. Shirman, M. Boterashvili, M. Orbach, D. Freeman, L. J. W. Shimon, M. Lahav and M. E. van der Boom, *Cryst. Growth Des.*, 2015, **15**, 4756-4759.
8. H. R. Khavasi and M. Esmaeili, *CrystEngComm*, 2014, **16**, 8479-8485.
9. P. Gómez, M. Más-Montoya, I. da Silva, J. P. Cerón-Carrasco, A. Tárraga and D. Curiel, *Cryst. Growth Des.*, 2017, **17**, 3371-3378.
10. X. Li, Y. Gao, R. Harniman, M. Winnik and I. Manners, *J. Am. Chem. Soc.*, 2016, **138**, 12902-12912.
11. Z. Gao, Y. Han, S. Chen, Z. Li, H. Tong and F. Wang, *ACS Macro Lett.*, 2017, **6**, 541-545.
12. H. Wang, Z. Bao, H. Wu, R.-B. Lin, W. Zhou, T.-L. Hu, B. Li, J. C.-G. Zhao and B. Chen, *Chem. Commun.*, 2017, **53**, 11150-11153.
13. A. Priimagi, G. Cavallo, P. Metrangolo and G. Resnati, *Acc. Chem. Res.*, 2013, **46**, 2686-2695.
14. M. C. Pfrunder, A. S. Micallef, L. Rintoul, D. P. Arnold and J. McMurtrie, *Cryst. Growth Des.*, 2016, **16**, 681-695.
15. R. Liu, H. Wang and W. J. Jin, *Cryst. Growth Des.*, 2017, **17**, 3331-3337.
16. J. Gamekkanda, A. Sinha, J. Desper, M. Đaković and C. Aakeröy, *Crystals*, 2017, **7**, 226.
17. D. Yan, D.-K. Bučar, A. Delori, B. Patel, G. O. Lloyd, W. Jones and X. Duan, *Chem. Eur. J.*, 2013, **19**, 8213-8219.
18. A. Vanderkooy and M. S. Taylor, *Faraday Discuss.*, 2017, **203**, 285-299.
19. C. B. Aakeröy, T. K. Wijethunga, J. Desper and M. Đaković, *Cryst. Growth Des.*, 2016, **16**, 2662-2670.
20. T. Clark, *Faraday Discuss.*, 2017, **203**, 9-27.
21. M. D. Perera, J. Desper, A. S. Sinha and C. B. Aakeröy, *CrystEngComm*, 2016, **18**, 8631-8636.
22. R. K. Rowe and P. S. Ho, *Acta Cryst. B*, 2017, **73**, 255-264.
23. C. A. Gunawardana, J. Desper, A. S. Sinha, M. Đaković and C. B. Aakeröy, *Faraday Discuss.*, 2017, **203**, 371-388.
24. C. C. Robertson, J. S. Wright, E. J. Carrington, R. N. Perutz, C. A. Hunter and L. Brammer, *Chem. Sci.*, 2017, **8**, 5392-5398.
25. I. D. H. Oswald, W. D. S. Motherwell and S. Parsons, *Acta Cryst. B*, 2005, **61**, 46-57.
26. R. B. Walsh, C. W. Padgett, P. Metrangolo, G. Resnati, T. W. Hanks and W. T. Pennington, *Cryst. Growth Des.*, 2001, **1**, 165-175.
27. E. Corradi, S. V. Meille, M. T. Messina, P. Metrangolo and G. Resnati, *Angew. Chem. Int. Ed.*, 2000, **39**, 1782-1786.
28. J.-L. Syssa-Magale, K. Boubekeur, P. Palvadeau, A. Meerschaut and B. Schollhorn, *CrystEngComm*, 2005, **7**, 302-308.
29. D. R. Weyna, T. Shattock, P. Vishweshwar and M. J. Zaworotko, *Cryst. Growth Des.*, 2009, **9**, 1106-1123.
30. C. B. Aakeröy, D. Welideniya and J. Desper, *CrystEngComm*, 2017, **19**, 11-13.
31. C. B. Aakeröy, C. L. Spartz, S. Dembowski, S. Dwyre and J. Desper, *IUCrJ*, 2015, **2**, 498-510.
32. R. Montis, M. Arca, M. C. Aragoni, A. Bauza, F. Demartin, A. Frontera, F. Isaia and V. Lippolis, *CrystEngComm*, 2017, **19**, 4401-4412.
33. Y. Geboes, F. De Proft and W. A. Herrebout, *Acta Cryst. B*, 2017, **73**, 168-178.
34. H. Ding, Y. Lu, W. Wu and H. Liu, *Chem. Phys.*, 2014, **441**, 30-37.
35. C. B. Aakeröy, S. Panikkattu, P. D. Chopade and J. Desper, *CrystEngComm*, 2013, **15**, 3125-3136.
36. O. Dumele, D. Wu, N. Trapp, N. Goroff and F. Diederich, *Org. Lett.*, 2014, **16**, 4722-4725.
37. C. B. Aakeröy, T. K. Wijethunga, J. Desper and M. Đaković, *Cryst. Growth Des.*, 2015, **15**, 3853-3861.
38. N. R. Goud, O. Bolton, E. C. Burgess and A. J. Matzger, *Cryst. Growth Des.*, 2016, **16**, 1765-1771.
39. *Spartan'14 Wavefunction, Inc., Irvine.*, 2013.

40. R. Hosseinzadeh, M. K. Abolfazli, M. Mohseni, M. Mohadjerani and Z. Lasemi, *J. Heterocycl. Chem.*, 2014, **51**, 1298-1305.
41. G. Cavallo, P. Mentrangolo, R. Milani, T. Pilati, A. Priimagi, G. Resnati and G. Terraneo, *Chem. Rev.*, 2016, **116**, 2478-2601.
42. A. Mukherjee, S. Tothadi and G. R. Desiraju, *Acc. Chem. Res.*, 2014, **47**, 2514-2524.
43. T. Steiner, *J. Chem. Soc., Chem. Commun.*, 1995, DOI: 10.1039/C39950000095, 95-96.
44. J. Joseph and E. D. Jemmis, *J. Am. Chem. Soc.*, 2007, **129**, 4620-4632.
45. L. González, N. Gimeno, R. M. Tejedor, V. Polo, M. B. Ros, S. Uriel and J. L. Serrano, *Chem. Mater.*, 2013, **25**, 4503-4510.
46. M. K. Corpinot, S. A. Stratford, M. Arhangelskis, J. Anka-Lufford, I. Halasz, N. Judas, W. Jones and D.-K. Bucar, *CrystEngComm*, 2016, **18**, 5434-5439.
47. M. Moradi, L. G. Tulli, J. Nowakowski, M. Baljovic, T. A. Jung and P. Shahgaldian, *Angew. Chem. Int. Ed.*, 2017, **56**, 14395-14399.
48. I. Avasthi, S. Khanna, S. K. Tripathi and S. Verma, *CrystEngComm*, 2017, **19**, 5202-5213.
49. E. Bosch, N. P. Bowling and J. Darko, *Cryst. Growth Des.*, 2015, **15**, 1634-1641.
50. E. Bosch, *Cryst. Growth Des.*, 2010, **10**, 3808-3813.
51. E. Bosch, *Acta Cryst. C*, 2016, **72**, 748-752.
52. C. R. Groom, I. J. Bruno, M. P. Lightfoot and S. C. Ward, *Acta Cryst. B*, 2016, **72**, 171-179.
53. D. K. Moss, J. D. Spence and M. H. Nantz, *J. Org. Chem.*, 1999, **64**, 4339-4343.



O-H hydrogen-bond donors and R-C≡C-I halogen-bond donors are close competitors for suitable nucleophilic sites in solid-state assembly.